Z. Angew. Math. Phys.

DOI 10.1007/s00033-014-0482-x

Zeitschrift für angewandte Mathematik und Physik ZAMP

A mode III arc-shaped crack with surface elasticity

Xu Wang

Abstract. We study the effect of surface elasticity on an arc-shaped crack in a linearly elastic isotropic homogeneous material under antiplane shear deformation. The surface mechanics is incorporated by using a continuum-based surface/interface model of Gurtin and Murdoch. We obtain a complete solution by reducing the problem to two decoupled first-order Cauchy-type singular integro-differential equations. It is shown that different from the case of a straight crack, the stresses exhibit both the weak logarithmic and the strong square root singularities at the tips of the arc crack.

Mathematics Subject Classification. 30E20 · 30E25 · 35Q74 · 45E05 · 74B05.

Keywords. Arc-shaped crack · Antiplane deformation · Surface elasticity · Conformal mapping · Logarithmic singularity · Square root singularity · Cauchy singular integro-differential equation.

1. Introduction

When the ratio of surface/interface area to volume becomes appreciable at the nanoscales, surface elasticity should be incorporated in the deformation analysis of nano-structured materials. One of the most successful theories of surface/interface elasticity is the Gurtin–Murdoch surface model proposed by Gurtin, Murdoch and co-workers [3–5]. The Gurtin–Murdoch model is equivalent to the assumption of a surface as a thin and stiff membrane perfectly bonded to the bulk material [2,13,16]. Among other applications, the Gurtin–Murdoch model has been incorporated into the analysis of crack problems [1,7–11]. It was conjectured very recently that the use of Gurtin–Murdoch model can suppress the traditional strong square root singularity to a weak logarithmic one [6,17]. In fact, the existence of the logarithmic singularity can be confirmed from the asymptotic behaviors of $\psi(\xi)$ near the crack tips obtained by [1]. A numerical justification of the logarithmic singularity can be found in [12].

So far, the Gurtin–Murdoch theory has only been used in the analysis of straight cracks. We notice that the curvature-dependent surface tension has been incorporated in the modeling of curvilinear plane strain cracks by using Muskhelishvili's complex variable method [18,19]. This work endeavors to study the contribution of the Gurtin–Murdoch surface elasticity to the antiplane deformation of an isotropic plane containing a mode III arc-shaped crack. The existence of nonzero curvature of the arc crack with surface effects will make the problem rather difficult to handle. In order to overcome this difficulty, we introduce a linear fractional transformation which conformally maps the arc crack onto a *straight* slit. The boundary value problem in the mapped plane can be formulated by considering a distribution of line dislocations and line forces on the straight slit. The problem is finally reduced to two decoupled first-order Cauchy singular integro-differential equations which can be numerically solved by using Chebyshev polynomials and a modified collocation method. Our analysis indicates that the stresses exhibit both the weak logarithmic and the strong square root singularities at the tips of the arc crack, which is quite different from the case of a mode III straight crack in which only the weak logarithmic singularity is present [6–8,17]. The existence of the additional square root singularity can be deduced from the asymptotic analysis for an interface crack under antiplane shear [15]. In this case, $\rho = 1/2$ is also a solution to Eq. (28) in [15] and will lead to the square root singularity.

Published online: 19 November 2014

2. Bulk and surface elasticity

2.1. The bulk elasticity

In a fixed rectangular coordinate system $x_i\,(i=1,\,2,\,3)$, let u_i, σ_{ij} and ε_{ij} be, respectively, the displacement, stress and strain in an isotropic elastic bulk material. The equilibrium equations and stress–strain law are

$$\sigma_{ij,j}=0,\quad \sigma_{ij}=2\mu\varepsilon_{ij}+\lambda\varepsilon_{kk}\delta_{ij},\quad \varepsilon_{ij}=\frac{1}{2}(u_{i,j}+u_{j,i}), \tag{1}$$

where λ and μ are Lame constants, δ_{ij} is the Kronecker delta.

For the antiplane shear deformation of an isotropic elastic material, the two shear stress components σ_{31} and σ_{32}, the out-of-plane displacement $w=u_3(x_1,x_2)$ and the stress function ϕ can be expressed in terms of a single analytic function $g(z)$ of the complex variable $z=x_1+\mathrm{i}x_2$ as

$$\sigma_{32}+\mathrm{i}\sigma_{31}=\mu g^{'}(z),\quad \mu^{-1}\phi+\mathrm{i}w=g(z). \tag{2}$$

In addition, the stress components can be expressed in terms of the stress function ϕ as

$$\sigma_{31}=-\phi_{,2},\quad \sigma_{32}=\phi_{,1}. \tag{3}$$

Let t and n be the tangential and normal directions of a curve Γ. Then, the stress components in the orthogonal coordinates formed by t and n are

$$\sigma_{3t}=-\frac{\partial\phi}{\partial n}=\mu\frac{\partial w}{\partial t},\quad \sigma_{3n}=\frac{\partial\phi}{\partial t}. \tag{4}$$

2.2. The surface elasticity

The equilibrium conditions on the surface incorporating interface/surface elasticity can be expressed as [3,5,14]

$$\begin{array}{ll}[\sigma_{\alpha j}n_j\underline{e}_\alpha]+\sigma^{\mathrm{s}}_{\alpha\beta,\beta}\underline{e}_\alpha=0, & \text{(tangential direction)}\\ [\sigma_{ij}n_in_j]=\sigma^{\mathrm{s}}_{\alpha\beta}\kappa_{\alpha\beta}, & \text{(normal direction)}\end{array} \tag{5}$$

where $\alpha,\,\beta=1,2$; n_i is the unit normal vector to the surface, $[*]$ denotes the jump of the quantities across the surface, $\sigma^{\mathrm{s}}_{\alpha\beta}$ is the surface stress tensor, and $\kappa_{\alpha\beta}$ is the curvature tensor of the surface. In addition, the constitutive equations on the isotropic surface are given by

$$\sigma^{\mathrm{s}}_{\alpha\beta}=\sigma_0\delta_{\alpha\beta}+2(\mu^{\mathrm{s}}-\sigma_0)\varepsilon^{\mathrm{s}}_{\alpha\beta}+(\lambda^{\mathrm{s}}+\sigma_0)\varepsilon^{\mathrm{s}}_{\gamma\gamma}\delta_{\alpha\beta}+\sigma_0\nabla_{\mathrm{s}}\mathbf{u}, \tag{6}$$

where $\varepsilon^{\mathrm{s}}_{\alpha\beta}$ is the surface strain tensor, σ_0 is the surface tension, λ^{s} and μ^{s} are the two surface Lame parameters, and ∇_{s} is the surface gradient.

3. A mode III arc-shaped crack with surface elasticity

Consider the antiplane shear deformation of a linearly elastic solid containing a mode III arc-shaped crack. The two crack tips are located at $z=\pm a$, and the midpoint of the arc crack is located at $z=\mathrm{i}h$, $(h>0)$, as shown in Fig. 1. The crack faces are traction free, and the solid is subjected to remote uniform antiplane shear stresses σ^{∞}_{31} and σ^{∞}_{32}.

It follows from Eq. (5) that the boundary conditions on the crack faces can be written as

$$\sigma^{\mathrm{s}}_{3t,t}+(\sigma_{3n})^{+}-(\sigma_{3n})^{-}=0,\quad \text{on the upper crack face,} \tag{7a}$$

$$\sigma^{\mathrm{s}}_{3t,t}+(\sigma_{3n})^{+}-(\sigma_{3n})^{-}=0,\quad \text{on the lower crack face,} \tag{7b}$$

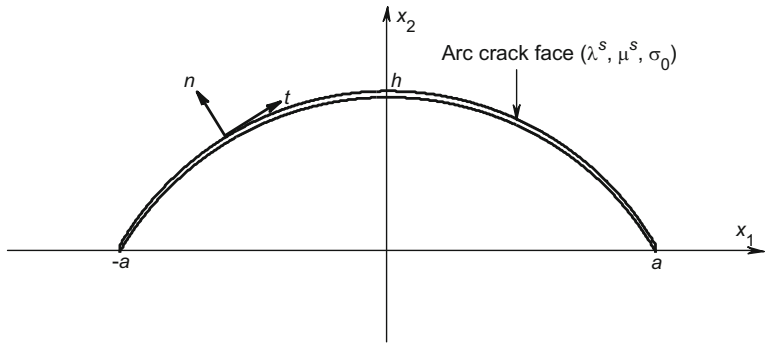

FIG. 1. Mode III arc-shaped crack with its two tips located at $z = \pm a$ and its midpoint at $z = \mathrm{i}h$.

where the subscripts t and n denote the tangential and normal directions of the arc crack as shown in Fig. 1, $(\sigma_{3n})^-$ in Eq. (7a) and $(\sigma_{3n})^+$ in Eq. (7b) are zero. By making use of Eq. (6) and assuming a coherent interface ($\varepsilon^{\mathrm{s}}_{\alpha\beta} = \varepsilon_{\alpha\beta}$), we can further express Eqs. (7a, 7b) into

$$(\sigma_{3n})^+ = -\left(\mu^{\mathrm{s}} - \sigma_0\right) u^+_{3,tt}, \quad \text{on the upper crack face,} \tag{8}$$

$$(\sigma_{3n})^- = \left(\mu^{\mathrm{s}} - \sigma_0\right) u^-_{3,tt}, \quad \text{on the lower crack face,} \tag{9}$$

which are equivalent to

$$\begin{aligned} (\sigma_{3n})^+ + (\sigma_{3n})^- &= -\left(\mu^{\mathrm{s}} - \sigma_0\right)\left(u^+_{3,tt} - u^-_{3,tt}\right), \\ (\sigma_{3n})^+ - (\sigma_{3n})^- &= -\left(\mu^{\mathrm{s}} - \sigma_0\right)\left(u^+_{3,tt} + u^-_{3,tt}\right). \end{aligned} \tag{10}$$

In order to solve the boundary value problem, we first introduce the following linear fractional mapping function

$$z = \omega(\xi) = \frac{a(a\xi + \mathrm{i}h)}{\mathrm{i}h\xi + a}, \quad \xi = \omega^{-1}(z) = \frac{a(h + \mathrm{i}z)}{hz + \mathrm{i}a^2}, \tag{11}$$

which conformally maps the arc-shaped crack in the physical z-plane onto a straight slit in the ξ-plane. More specifically, the two crack tips $z = \pm a$ are mapped onto the two tips $\xi = \pm 1$ of the slit, the midpoint of the arc crack $z = \mathrm{i}h$ is mapped to $\xi = 0$, and $z = \infty$ is mapped to $\xi = \mathrm{i}a/h$. It is more convenient to discuss the problem in the ξ-plane because the slit just lies on the real axis in the ξ-plane. In the following analysis, let $g(\xi) = g(\omega(\xi)) = g(z)$.

We can formulate the boundary value problem in the ξ-plane by considering a distribution of line dislocations with density $a \cdot b(\xi)$ and line forces with density $a \cdot f(\xi)$ on the straight slit $-1 \le \mathrm{Re}\{\xi\} \le 1$, $\mathrm{Im}\{\xi\} = 0$. Consequently, the analytic function $g(\xi)$ can be written into the following form

$$g(\xi) = \frac{a}{2\pi}\int_{-1}^{1}\left[b(\eta) - \mathrm{i}\mu^{-1}f(\eta)\right]\ln\left(\frac{\xi - \eta}{\mathrm{i}h\xi + a}\right)\mathrm{d}\eta + \frac{\sigma^{\infty}_{32} + \mathrm{i}\sigma^{\infty}_{31}}{\mu}\omega(\xi). \tag{12}$$

By using the following auxiliary conditions which will be proved later,

$$\int_{-1}^{1} b(\eta)\mathrm{d}\eta = 0, \quad \int_{-1}^{1} f(\eta)\mathrm{d}\eta = 0, \tag{13}$$

Equation (12) simplifies to

$$g(\xi) = \frac{a}{2\pi}\int_{-1}^{1}\left[b(\eta) - \mathrm{i}\mu^{-1}f(\eta)\right]\ln(\xi - \eta)\mathrm{d}\eta + \frac{\sigma^{\infty}_{32} + \mathrm{i}\sigma^{\infty}_{31}}{\mu}\omega(\xi). \tag{14}$$

It is deduced from the above expression that

$$g_{+}^{'}(\xi)=-\frac{a\left[\mathrm{i}b(\xi)+\mu^{-1}f(\xi)\right]}{2}+\frac{a}{2\pi}\int_{-1}^{1}\frac{b(\eta)-\mathrm{i}\mu^{-1}f(\eta)}{\xi-\eta}\mathrm{d}\eta+\frac{\sigma_{32}^{\infty}+\mathrm{i}\sigma_{31}^{\infty}}{\mu}\frac{a(a^2+h^2)}{(\mathrm{i}h\xi+a)^2}, \tag{15}$$

$$g_{-}^{'}(\xi)=\frac{a\left[\mathrm{i}b(\xi)+\mu^{-1}f(\xi)\right]}{2}+\frac{a}{2\pi}\int_{-1}^{1}\frac{b(\eta)-\mathrm{i}\mu^{-1}f(\eta)}{\xi-\eta}\mathrm{d}\eta+\frac{\sigma_{32}^{\infty}+\mathrm{i}\sigma_{31}^{\infty}}{\mu}\frac{a(a^2+h^2)}{(\mathrm{i}h\xi+a)^2}, \tag{16}$$

where the subscript "+" means the limiting value by approaching the slit from the upper half plane, the subscript "−" means the limiting value by approaching the slit from the lower half plane.

By imposing the boundary conditions in Eq. (10) and making use of Eq. (4), we obtain the following hyper-singular integro-differential equations

$$-\frac{1}{\pi}\int_{-1}^{1}\frac{\hat{b}(\eta)}{\eta-\xi}\mathrm{d}\eta+2(1+\hat{h}^2)\mathrm{Re}\left\{\frac{e^{\mathrm{i}\psi}}{(\mathrm{i}\hat{h}\xi+1)^2}\right\}=\frac{S_e}{1+\hat{h}^2}\left[2\hat{h}^2\xi\hat{b}(\xi)+(1+\hat{h}^2\xi^2)\hat{b}^{'}(\xi)\right],\quad -1<\xi<1, \tag{17}$$

$$\frac{1+\hat{h}^2\xi^2}{\pi(1+\hat{h}^2)}\int_{-1}^{1}\frac{\hat{f}(\eta)}{(\xi-\eta)^2}\mathrm{d}\eta-\frac{2\hat{h}^2\xi}{\pi(1+\hat{h}^2)}\int_{-1}^{1}\frac{\hat{f}(\eta)}{\xi-\eta}\mathrm{d}\eta-\frac{1}{S_e}\hat{f}(\xi)=4\hat{h}\mathrm{Re}\left\{\frac{e^{\mathrm{i}\psi}}{(\mathrm{i}\hat{h}\xi+1)^2}\right\},\quad -1<\xi<1, \tag{18}$$

where

$$\begin{aligned}&S_e=\frac{\mu^s-\sigma_0}{a\mu},\\&\hat{h}=\frac{h}{a},\quad \hat{b}(\xi)=\frac{\mu b(\xi)}{T},\quad \hat{f}(\xi)=\frac{f(\xi)}{T},\\&\sigma_{32}^{\infty}+\mathrm{i}\sigma_{31}^{\infty}=Te^{\mathrm{i}\psi},\end{aligned} \tag{19}$$

with T and ψ the magnitude and phase angle of $\sigma_{32}^{\infty}+\mathrm{i}\sigma_{31}^{\infty}$.

More precisely, Eq. (17) is a Cauchy singular integro-differential equation, whereas Eq. (18) is a hyper-singular integral equation.

Equation (17) is equivalent to

$$\int_{-1}^{1}\frac{I(\eta)}{\eta-\xi}\mathrm{d}\eta=-\frac{\pi S_e}{1+\hat{h}^2}(1+\hat{h}^2\xi^2)I^{'}(\xi)-2\pi(1+\hat{h}^2)\xi\mathrm{Re}\left\{\frac{e^{\mathrm{i}\psi}}{\mathrm{i}\hat{h}\xi+1}\right\}-\pi k,\quad -1<\xi<1, \tag{20}$$

where k is an unknown real constant to be determined, and

$$I(\xi)=-\int_{-1}^{\xi}\hat{b}(\eta)\mathrm{d}\eta. \tag{21}$$

Equation (18) is equivalent to

$$\frac{1+\hat{h}^2\xi^2}{\pi(1+\hat{h}^2)}\int_{-1}^{1}\frac{\hat{f}(\eta)}{\eta-\xi}\mathrm{d}\eta-\frac{1}{S_e}\int_{-1}^{\xi}\hat{f}(\eta)\mathrm{d}\eta=4\hat{h}\xi\mathrm{Re}\left\{\frac{e^{\mathrm{i}\psi}}{\mathrm{i}\hat{h}\xi+1}\right\}-2\sin\psi,\quad -1<\xi<1. \tag{22}$$

It is simply deduced that

$$\Delta w = w^+ - w^- = -a\int_{-1}^{\xi} b(\eta)\mathrm{d}\eta = \frac{aT}{\mu}I(\xi), \quad \sigma_{3n}^+ - \sigma_{3n}^- = -\frac{af(\xi)}{|\omega'(\xi)|}, \quad -1 < \xi < 1. \tag{23}$$

Thus, the single valuedness of the displacement and balance of force for a contour surrounding the crack surface will lead to the conditions in Eq. (13).

The original boundary value problem has now been reduced to two decoupled first-order Cauchy singular integro-differential equations in Eqs. (20) and (22) with the following auxiliary conditions

$$I(-1) = I(1) = 0, \tag{24}$$

$$\int_{-1}^{1} \hat{f}(\eta)\mathrm{d}\eta = 0. \tag{25}$$

4. Solution to the singular integro-differential equations

By using the inverse operator T^{-1} defined below to Eq. (20),

$$T^{-1}\psi(\xi) = \frac{1}{\pi\sqrt{1-\xi^2}}\int_{-1}^{1}\psi(\eta)\mathrm{d}\eta - \frac{1}{\pi^2\sqrt{1-\xi^2}}\int_{-1}^{1}\frac{\sqrt{1-\eta^2}\psi(\eta)}{\eta-\xi}\mathrm{d}\eta, \quad -1 < \xi < 1, \tag{26}$$

we obtain

$$\sqrt{1-\xi^2}I(\xi) = \frac{1}{\pi}\int_{-1}^{1} I(\eta)\mathrm{d}\eta + \frac{1}{\pi}\int_{-1}^{1}\frac{\sqrt{1-\eta^2}\left[\frac{S_e}{1+\hat{h}^2}(1+\hat{h}^2\eta^2)I'(\eta) + 2(1+\hat{h}^2)\eta\mathrm{Re}\left\{\frac{e^{\mathrm{i}\psi}}{\mathrm{i}\hat{h}\eta+1}\right\} + k\right]}{\eta-\xi}\mathrm{d}\eta,$$
$$-1 < \xi < 1, \tag{27}$$

The two unknown functions $I(\xi)$ and $\hat{f}(\xi)$ are approximated as

$$I(\xi) = \sum_{m=0}^{N} c_m T_m(\xi), \tag{28}$$

$$\hat{f}(\xi) = \frac{1}{\sqrt{1-\xi^2}}\sum_{m=0}^{N} d_m T_m(\xi), \tag{29}$$

where $T_m(\xi)$ represents the mth Chebyshev polynomial of the first kind. It is observed that $I(\xi)$ is finite at $\xi = \pm 1$, whereas $\hat{f}(\xi)$ exhibits square root singularity at $\xi = \pm 1$.

Substituting Eq. (28) into Eq. (27) and utilizing the following identities

$$\frac{\mathrm{d}T_m(\xi)}{\mathrm{d}\xi} = mU_{m-1}(\xi), \tag{30}$$

$$4\xi^2 U_m(\xi) = \begin{cases} U_{m+2}(\xi) + U_m(\xi), & m = 0 \\ U_{m+2}(\xi) + 2U_m(\xi), & m = 1 \\ U_{m+2}(\xi) + 2U_m(\xi) + U_{m-2}(\xi), & m > 1 \end{cases} \tag{31}$$

$$\int_{-1}^{1} T_m(\eta)\mathrm{d}\eta = \begin{cases} \frac{1+(-1)^m}{1-m^2}, & m \neq 1, \\ 0, & m = 1, \end{cases} \tag{32}$$

$$\int_{-1}^{1} \frac{U_m(\eta)\sqrt{1-\eta^2}}{\eta-\xi}\mathrm{d}\eta = -\pi T_{m+1}(\xi), \tag{33}$$

$$\int_{-1}^{1} \frac{\eta\sqrt{1-\eta^2}}{(\eta-\xi)(\mathrm{i}\hat{h}\eta+1)}\mathrm{d}\eta = \frac{1}{1+\mathrm{i}\hat{h}\xi}\left(\xi\int_{-1}^{1}\frac{\sqrt{1-\eta^2}}{\eta-\xi}\mathrm{d}\eta + \int_{-1}^{1}\frac{\sqrt{1-\eta^2}}{\mathrm{i}\hat{h}\eta+1}\mathrm{d}\eta\right)$$
$$= \frac{\pi}{1+\mathrm{i}\hat{h}\xi}\left(-\xi^2+\frac{\sqrt{1+\hat{h}^2}-1}{\hat{h}^2}\right), \tag{34}$$

with $U_m(x)$ being the mth Chebyshev polynomial of the second kind, we can finally arrive at

$$\sum_{m=0}^{N} c_m T_m(\xi)\left(\sqrt{1-\xi^2}+\frac{S_e m}{1+\hat{h}^2}\right)$$
$$+\frac{S_e\hat{h}^2}{4(1+\hat{h}^2)}\left\{c_1\left[T_1(\eta)+T_3(\eta)\right]+2c_2\left[2T_2(\eta)+T_4(\eta)\right]+\sum_{m=3}^{N} m c_m\left[T_{m+2}(\eta)+2T_m(\eta)+T_{m-2}(\eta)\right]\right\}$$
$$-\sum_{m=0,m\neq 1}^{N}\frac{1+(-1)^m}{\pi(1-m^2)}c_m + k\xi = 2(1+\hat{h}^2)\left(-\xi^2+\frac{\sqrt{1+\hat{h}^2}-1}{\hat{h}^2}\right)\mathrm{Re}\left\{\frac{e^{\mathrm{i}\psi}}{1+\mathrm{i}\hat{h}\xi}\right\}. \tag{35}$$

Substituting Eq. (29) into Eq. (22), utilizing the following identities

$$\int_{-1}^{1}\frac{T_m(\eta)}{(\eta-\xi)\sqrt{1-\eta^2}}\mathrm{d}\eta = \pi U_{m-1}(\xi), \tag{36}$$

and performing the incomplete integrals, we arrive at

$$\frac{1}{S_e}d_0(\cos^{-1}\xi-\pi)+\sum_{m=1}^{N} d_m\left[\frac{(1+\hat{h}^2\xi^2)U_{m-1}(\xi)}{1+\hat{h}^2}+\frac{1}{S_e m}\sin(m\cos^{-1}\xi)\right] = 4\hat{h}\xi\mathrm{Re}\left\{\frac{e^{\mathrm{i}\psi}}{\mathrm{i}\hat{h}\xi+1}\right\}-2\sin\psi. \tag{37}$$

If we select the collocation points given by $\xi = -\cos\left(\frac{i\pi}{N}\right)$ for $i = 1, 2, \ldots, N$, Eqs. (35), (24), (37) and (25) reduce to the following sets of linear algebraic equations

$$\sum_{m=0}^{N}(-1)^m c_m\cos\left(\frac{mi\pi}{N}\right)\left[\sqrt{1-\left(\cos\left(\frac{i\pi}{N}\right)\right)^2}+\frac{S_e m}{1+\hat{h}^2}\right]$$
$$+\frac{S_e\hat{h}^2}{4(1+\hat{h}^2)}\left\{\begin{array}{l}-c_1\left[\cos\left(\frac{i\pi}{N}\right)+\cos\left(\frac{3i\pi}{N}\right)\right]+2c_2\left[2\cos\left(\frac{2i\pi}{N}\right)+\cos\left(\frac{4i\pi}{N}\right)\right]\\ +\sum_{m=3}^{N}(-1)^m m c_m\left[\cos\left(\frac{i(m+2)\pi}{N}\right)+2\cos\left(\frac{mi\pi}{N}\right)+\cos\left(\frac{i(m-2)\pi}{N}\right)\right]\end{array}\right\}$$
$$-\sum_{m=0,m\neq 1}^{N}\frac{1+(-1)^m}{\pi(1-m^2)}c_m - k\cos\left(\frac{i\pi}{N}\right)$$
$$= 2(1+\hat{h}^2)\left[-\left(\cos\left(\frac{i\pi}{N}\right)\right)^2+\frac{\sqrt{1+\hat{h}^2}-1}{\hat{h}^2}\right]\frac{\cos\psi-\hat{h}\cos\left(\frac{i\pi}{N}\right)\sin\psi}{1+\hat{h}^2\left(\cos\left(\frac{i\pi}{N}\right)\right)^2},\quad i=1,2,\ldots,N,$$
$$\sum_{m=0}^{N} c_m = 0,\quad \sum_{m=0}^{N}(-1)^m c_m = 0, \tag{38}$$

$$
\begin{aligned}
&-\frac{d_0}{S_e}\frac{i\pi}{N}+\sum_{m=1}^{N}(-1)^{m-1}\sin\left(\frac{mi\pi}{N}\right)\left[\frac{1+\hat{h}^2\left(\cos\left(\frac{i\pi}{N}\right)\right)^2}{1+\hat{h}^2}\frac{1}{\sin\left(\frac{i\pi}{N}\right)}+\frac{1}{S_e m}\right]d_m\\
&=-4\hat{h}\cos\left(\frac{i\pi}{N}\right)\frac{\cos\psi-\hat{h}\cos\left(\frac{i\pi}{N}\right)\sin\psi}{1+\hat{h}^2\left(\cos\left(\frac{i\pi}{N}\right)\right)^2}-2\sin\psi,\quad i=1,2,\ldots,N-1,\\
&-\frac{d_0}{S_e}\pi+\sum_{m=1}^{N}md_m=4\hat{h}\frac{\cos\psi+\hat{h}\sin\psi}{1+\hat{h}^2}-2\sin\psi,\\
&d_0=0.
\end{aligned}
\tag{39}
$$

The $(N+2)$ unknowns c_m, $(m=0,1,2,\ldots,N)$ and k can be uniquely determined by solving Eq. (38) which contains $(N+2)$ independent equations, the other $(N+1)$ unknowns d_m, $(m=0,1,2,\ldots,N)$ can be uniquely determined by solving Eq. (39) which contains $(N+1)$ independent equations.

5. The stress field

By substituting the following expression of $\frac{g'(\xi)}{\omega'(\xi)}$ into Eq. (2)

$$
\frac{g'(\xi)}{\omega'(\xi)}=\frac{T(i\hat{h}\xi+1)^2}{2\pi\mu(1+\hat{h}^2)}\int_{-1}^{1}\frac{-I'(\eta)-i\hat{f}(\eta)}{\xi-\eta}d\eta+\frac{\sigma_{32}^{\infty}+i\sigma_{31}^{\infty}}{\mu},
\tag{40}
$$

we arrive at the full-field stress field as

$$
\sigma_{32}+i\sigma_{31}=\frac{T(i\hat{h}\xi+1)^2}{2\pi(1+\hat{h}^2)}\int_{-1}^{1}\frac{-I'(\eta)-i\hat{f}(\eta)}{\xi-\eta}d\eta+\sigma_{32}^{\infty}+i\sigma_{31}^{\infty}.
\tag{41}
$$

σ_{3n} and σ_{3t} are distributed along the circle $\left|z+\frac{a^2-h^2}{2h}i\right|=\frac{a^2+h^2}{2h}$ where the arc crack is located as follows:

$$
\begin{aligned}
\sigma_{3n}&=\frac{T(1+\hat{h}^2\xi^2)}{2\pi(1+\hat{h}^2)}\int_{-1}^{1}\frac{I'(\eta)}{\eta-\xi}d\eta+\frac{(1-\hat{h}^2\xi^2)\sigma_{32}^{\infty}+2\hat{h}\xi\sigma_{31}^{\infty}}{1+\hat{h}^2\xi^2},\quad \xi<-1\text{or }\xi>1,\\
\sigma_{3t}&=\frac{T(1+\hat{h}^2\xi^2)}{2\pi(1+\hat{h}^2)}\int_{-1}^{1}\frac{\hat{f}(\eta)}{\eta-\xi}d\eta+\frac{(1-\hat{h}^2\xi^2)\sigma_{31}^{\infty}-2\hat{h}\xi\sigma_{32}^{\infty}}{1+\hat{h}^2\xi^2},\quad \xi<-1\text{ or }\xi>1,
\end{aligned}
\tag{42}
$$

$$
\begin{aligned}
(\sigma_{3n})^{+}&=-\frac{TS_e(1+\hat{h}^2\xi^2)}{2(1+\hat{h}^2)^2}\left[2\hat{h}^2\xi I'(\xi)+(1+\hat{h}^2\xi^2)I''(\xi)\right]-\frac{T(1+\hat{h}^2\xi^2)}{2(1+\hat{h}^2)}\hat{f}(\xi),\\
(\sigma_{3n})^{-}&=-\frac{TS_e(1+\hat{h}^2\xi^2)}{2(1+\hat{h}^2)^2}\left[2\hat{h}^2\xi I'(\xi)+(1+\hat{h}^2\xi^2)I''(\xi)\right]+\frac{T(1+\hat{h}^2\xi^2)}{2(1+\hat{h}^2)}\hat{f}(\xi),
\end{aligned}
\qquad -1<\xi<1,
\tag{43}
$$

$$
\begin{aligned}
(\sigma_{3t})^{+}&=\frac{T}{2S_e}\int_{-1}^{\xi}\hat{f}(\eta)d\eta+\frac{T(1+\hat{h}^2\xi^2)}{2(1+\hat{h}^2)}I'(\xi),\\
(\sigma_{3t})^{-}&=\frac{T}{2S_e}\int_{-1}^{\xi}\hat{f}(\eta)d\eta-\frac{T(1+\hat{h}^2\xi^2)}{2(1+\hat{h}^2)}I'(\xi),
\end{aligned}
\qquad -1<\xi<1.
\tag{44}
$$

Because $\frac{g'(\xi)}{\omega'(\xi)}$ exhibits the following singular behaviors at $\xi=\pm1$

$$\frac{g^{'}(\xi)}{\omega^{'}(\xi)}=\frac{T}{2\pi\mu}\frac{1+\mathrm{i}\hat{h}}{1-\mathrm{i}\hat{h}}\left(\sum_{m=0}^{N}m^2c_m\right)\ln(\xi-1)-\frac{\mathrm{i}T}{2\sqrt{2}\mu}\frac{1+\mathrm{i}\hat{h}}{1-\mathrm{i}\hat{h}}\left(\sum_{m=0}^{N}d_m\right)\frac{1}{\sqrt{\xi-1}}+O(1),\quad \text{as } \xi\to 1,$$

$$\begin{aligned}\frac{g^{'}(\xi)}{\omega^{'}(\xi)}=&\frac{T}{2\pi\mu}\frac{1-\mathrm{i}\hat{h}}{1+\mathrm{i}\hat{h}}\left(\sum_{m=0}^{N}(-1)^m m^2c_m\right)\ln(\xi+1)\\&-\frac{T}{2\sqrt{2}\mu}\frac{1-\mathrm{i}\hat{h}}{1+\mathrm{i}\hat{h}}\left(\sum_{m=0}^{N}(-1)^m d_m\right)\frac{1}{\sqrt{\xi+1}}+O(1),\quad \text{as } \xi\to -1,\end{aligned}\tag{45}$$

the stress components σ_{31} and σ_{32} exhibit both the weak logarithmic and the strong square root singularities at the two crack tips $z=\pm a$, which is quite different from the case of a mode III straight crack in which only the weak logarithmic singularity is present [6–8,17].

It is further deduced from Eqs. (42), (28) and (29) that the two stress components σ_{3n} and σ_{3t} are singularly distributed near the two crack tips as

$$\begin{aligned}
&\sigma_{3n}=\tfrac{T}{2\pi}\left(\sum_{m=0}^{N}m^2c_m\right)\ln(\xi-1)+O(1), && \text{as } \xi-1\to 0^+,\\
&\sigma_{3t}=-\tfrac{T}{2\sqrt{2}}\left(\sum_{m=0}^{N}d_m\right)\tfrac{1}{\sqrt{\xi-1}}+O(1), && \text{as } \xi-1\to 0^+,\\
&(\sigma_{3n})^+=-(\sigma_{3n})^-=-\tfrac{T}{2\sqrt{2}}\left(\sum_{m=0}^{N}d_m\right)\tfrac{1}{\sqrt{1-\xi}}+O(1), && \text{as } \xi-1\to 0^-,\\
&(\sigma_{3t})^+=O(1),\quad (\sigma_{3t})^-=O(1), && \text{as } \xi-1\to 0^-,\\
&\sigma_{3n}=\tfrac{T}{2\pi}\left(\sum_{m=0}^{N}(-1)^m m^2c_m\right)\ln|\xi+1|+O(1), && \text{as } \xi+1\to 0^-,\\
&\sigma_{3t}=\tfrac{T}{2\sqrt{2}}\left(\sum_{m=0}^{N}(-1)^m d_m\right)\tfrac{1}{\sqrt{|\xi+1|}}+O(1), && \text{as } \xi+1\to 0^-,\\
&(\sigma_{3n})^+=-(\sigma_{3n})^-=-\tfrac{T}{2\sqrt{2}}\left(\sum_{m=0}^{N}(-1)^m d_m\right)\tfrac{1}{\sqrt{1+\xi}}+O(1), && \text{as } \xi+1\to 0^+,\\
&(\sigma_{3t})^+=O(1),\quad (\sigma_{3t})^-=O(1), && \text{as } \xi+1\to 0^+.
\end{aligned}\tag{46}$$

It is observed from the above expression that σ_{3n} outside the crack only exhibits the weak logarithmic singularity, σ_{3n} on the crack faces only exhibits the strong square root singularity; whereas σ_{3t} outside the crack only exhibits the strong square root singularity, σ_{3t} is bounded everywhere on the crack faces.

6. Numerical results and discussion

It is observed from the analysis in Sect. 5 that the complete stress field can be obtained once the two functions $I(\xi)$ and $\hat{f}(\xi)$ are determined. In this section, we first present the closed-form expressions of $I(\xi)$ and $\hat{f}(\xi)$ for the two extreme cases $S_e=0$ and $S_e\to\infty$. Then, we illustrate our numerical results of $I(\xi)$ and $\hat{f}(\xi)$ obtained by solving Eqs. (38) and (39) and compare the numerical results with the exact solutions for $S_e=0$ and $S_e\to\infty$.

6.1. The classical solutions

When $S_e=0$, the following exact solution can be derived

$$g(\xi)=\frac{1}{2}\frac{aT}{\mu}\frac{1+\hat{h}^2}{\hat{h}^2}\left[\frac{e^{\mathrm{i}\psi}}{\xi-\frac{\mathrm{i}}{\hat{h}}}-\frac{e^{-\mathrm{i}\psi}}{\xi+\frac{\mathrm{i}}{\hat{h}}}+\frac{e^{\mathrm{i}\psi}\sqrt{\xi^2-1}}{\mathrm{i}\sqrt{\frac{1}{\hat{h}^2}+1}\left(\xi-\frac{\mathrm{i}}{\hat{h}}\right)}-\frac{e^{-\mathrm{i}\psi}\sqrt{\xi^2-1}}{\mathrm{i}\sqrt{\frac{1}{\hat{h}^2}+1}\left(\xi+\frac{\mathrm{i}}{\hat{h}}\right)}\right].\tag{47}$$

It is simply derived from the above expression that

$$\Delta w = \frac{2aT}{\mu}\sqrt{1+\hat{h}^2}\sqrt{1-\xi^2}\mathrm{Im}\left\{\frac{e^{\mathrm{i}\psi}}{\hat{h}\xi-\mathrm{i}}\right\}, \quad \Delta\phi = 0, \quad -1<\xi<1. \tag{48}$$

A comparison of Eq. (48) with Eq. (23) leads to the following closed-from expressions of $I(\xi)$ and $\hat{f}(\xi)$

$$I(\xi) = 2\sqrt{1+\hat{h}^2}\sqrt{1-\xi^2}\mathrm{Im}\left\{\frac{e^{\mathrm{i}\psi}}{\hat{h}\xi-\mathrm{i}}\right\}, \quad \hat{f}(\xi) = 0, \quad -1<\xi<1. \tag{49}$$

On the other extreme end, when $S_e \to \infty$, the crack becomes a rigid line inclusion. In this case, the following exact solution can be derived

$$g(\xi) = \frac{1}{2}\frac{aT}{\mu}\frac{1+\hat{h}^2}{\hat{h}^2}\left[\frac{e^{\mathrm{i}\psi}}{\xi-\frac{\mathrm{i}}{\hat{h}}}+\frac{e^{-\mathrm{i}\psi}}{\xi+\frac{\mathrm{i}}{\hat{h}}}+\frac{e^{\mathrm{i}\psi}\sqrt{\xi^2-1}}{\mathrm{i}\sqrt{\frac{1}{\hat{h}^2}+1}\left(\xi-\frac{\mathrm{i}}{\hat{h}}\right)}+\frac{e^{-\mathrm{i}\psi}\sqrt{\xi^2-1}}{\mathrm{i}\sqrt{\frac{1}{\hat{h}^2}+1}\left(\xi+\frac{\mathrm{i}}{\hat{h}}\right)}\right]. \tag{50}$$

It is simply derived from the above expression that

$$\Delta w = 0, \quad \Delta\phi = 2aT\sqrt{1+\hat{h}^2}\sqrt{1-\xi^2}\mathrm{Re}\left\{\frac{e^{\mathrm{i}\psi}}{\hat{h}\xi-\mathrm{i}}\right\}, \quad -1<\xi<1. \tag{51}$$

A comparison of Eq. (51) with Eq. (23) leads to the following closed-from expressions of $I(\xi)$ and $\hat{f}(\xi)$

$$I(\xi) = 0, \quad \hat{f}(\xi) = \frac{2\sqrt{1+\hat{h}^2}}{\sqrt{1-\xi^2}}\mathrm{Re}\left\{\frac{e^{\mathrm{i}\psi}(-\mathrm{i}\xi+\hat{h})}{(\hat{h}\xi-\mathrm{i})^2}\right\}, \quad -1<\xi<1. \tag{52}$$

6.2. Numerical results

We illustrate in Figs. 2 and 3 the distributions of $I(\xi)$ and $\hat{f}(\xi)$ for different values of $\hat{h}$ with $S_e = 1$ and ψ=0 (or equivalently $\sigma_{31}^{\infty} = 0$). It is observed that when $\hat{h} = 0$, $I(\xi)$ is just the result for a straight crack, and meanwhile, $\hat{f}(\xi) \equiv 0$. Both $I(\xi)$ and $\hat{f}(\xi)$ are even functions of ξ when $\psi = 0$. The parameter $\hat{h}$ exerts

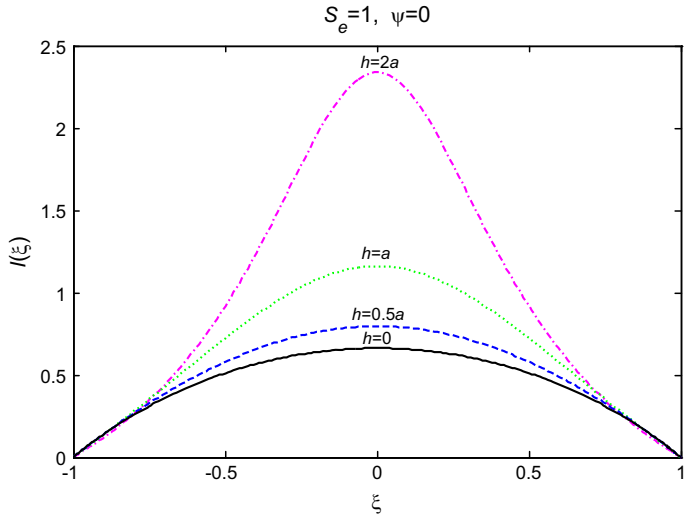

FIG. 2. Distribution of $I(\xi)$ for different values of $\hat{h}$ with $S_e = 1$ and ψ=0.

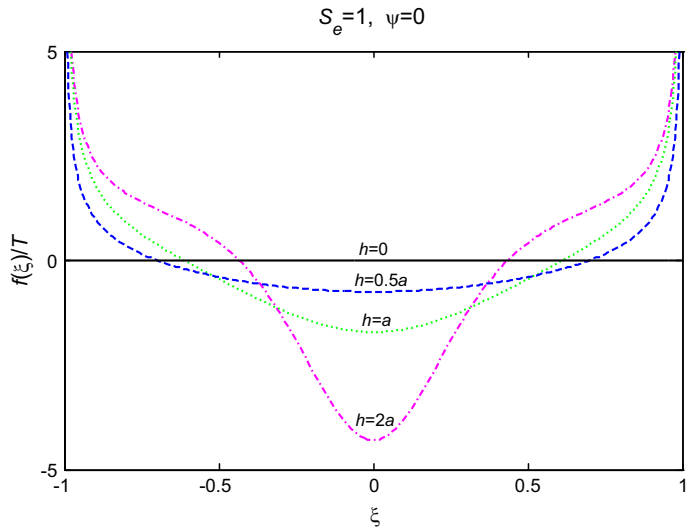

FIG. 3. Distribution of $\hat{f}(\xi)$ for different values of $\hat{h}$ with $S_e = 1$ and ψ=0.

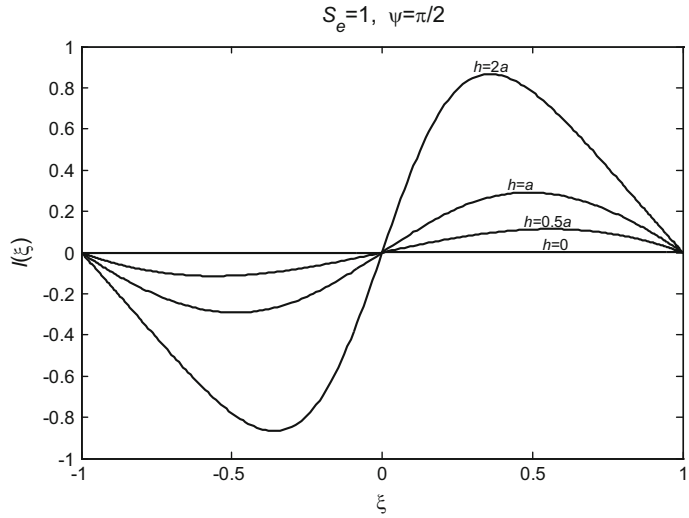

FIG. 4. Distribution of $I(\xi)$ for different values of $\hat{h}$ with $S_e = 1$ and $\psi = \pi/2$.

a significant influence on both $I(\xi)$ and $\hat{f}(\xi)$. Because $\frac{\partial \Delta w}{\partial t} = \frac{1}{|\omega'(\xi)|}\frac{\partial \Delta w}{\partial \xi} = \frac{aT}{\mu}\frac{I'(\xi)}{|\omega'(\xi)|}$ and $\left|\omega'(\pm 1)\right| = a$, we have at the two crack tips that $\frac{\partial \Delta w}{\partial t} = \frac{T}{\mu} I'(\pm 1)$. This result implies that the crack-tip opening angle can be simply determined by $I'(\pm 1)$. Consequently, it is observed from Fig. 2 that the crack-tip opening angles for different values of $\hat{h}$ with S_e being fixed are very close and are less than $\pi/2$. As observed in Fig. 3, $\hat{f}(\xi)$ is nonzero for an arc-shaped crack with $\hat{h} \neq 0$. This fact implies that both line dislocation and line force solutions are needed to simulate an arc crack with surface elasticity. Illustrated in Figs. 4 and 5 are distributions of $I(\xi)$ and $\hat{f}(\xi)$ for different values of $\hat{h}$ with $S_e = 1$ and $\psi = \pi/2$ (or equivalently $\sigma_{32}^{\infty} = 0$). It is observed from the two figures that (i) $I(\xi)$ and $\hat{f}(\xi)$ are odd functions of ξ; (ii) $I(\xi) \equiv 0$,

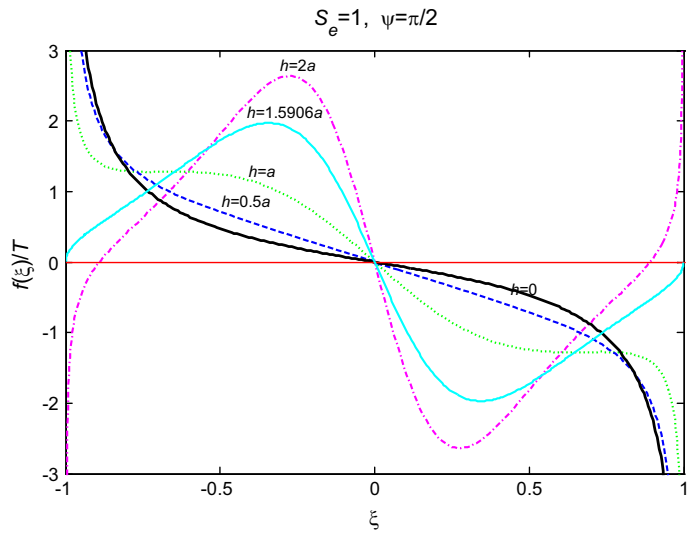

FIG. 5. Distribution of $\hat{f}(\xi)$ for different values of $\hat{h}$ with $S_e = 1$ and $\psi = \pi/2$.

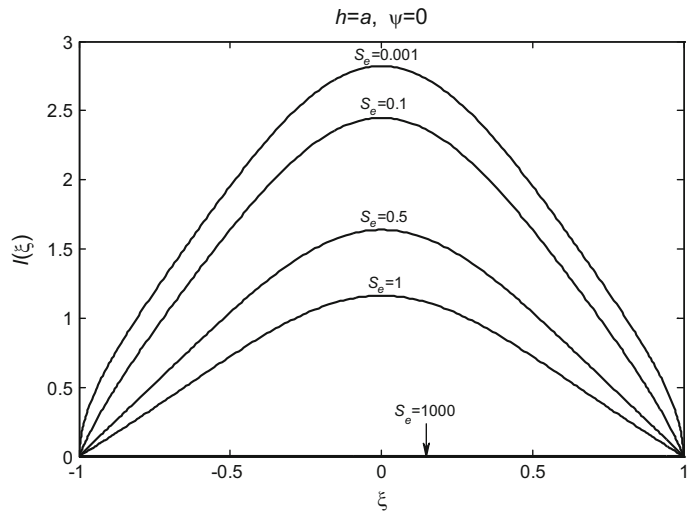

FIG. 6. Distribution of $I(\xi)$ for different values of S_e with $\hat{h} = 1$ and ψ=0.

whereas $\hat{f}(\xi) \neq 0$ when $\hat{h} = 0$; (iii) the crack-tip opening angle is an increasing function of $\hat{h}$ and is less than $\pi/2$; and (iv) the geometric parameter $\hat{h}$ exerts a significant influence on the distribution of both $I(\xi)$ and $\hat{f}(\xi)$. In particular, $\hat{f}(\pm 1) = 0$ when $\hat{h} = 1.5906$ as shown in Fig. 5. This fact implies that the stresses only exhibit the weak logarithmic singularity at the two crack tips under the loading phase angle of $\psi = \pi/2$ for some judicially chosen values of $\hat{h}$ and S_e.

Figures 6, 7, 8, 9 show the distributions of $I(\xi)$ and $\hat{f}(\xi)$ for different values of S_e with $\hat{h} = 1$ and $\psi = 0, \pi/2$. It is observed that an increase in S_e will suppress the magnitude of $I(\xi)$, or equivalently the crack opening displacement Δw (see Eq. (23)) and meanwhile enhance the magnitude of $\hat{f}(\xi)$. It is observed from Figs. 6 and 8 that the crack-tip opening angle is a decreasing function of S_e and that it

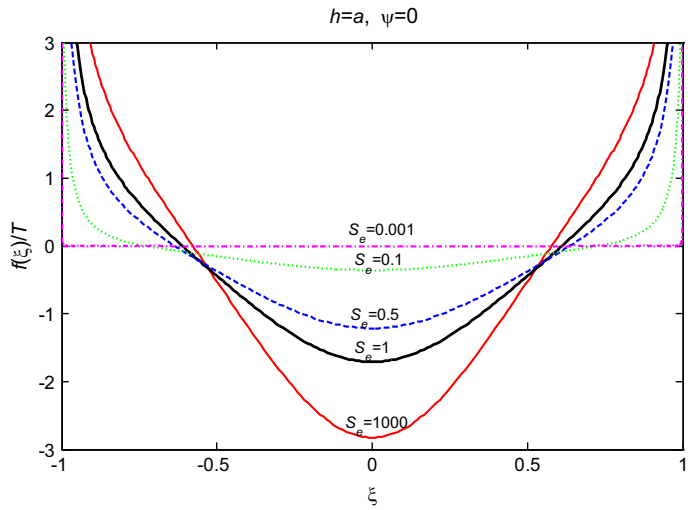

FIG. 7. Distribution of $\hat{f}(\xi)$ for different values of S_e with $\hat{h} = 1$ and ψ=0.

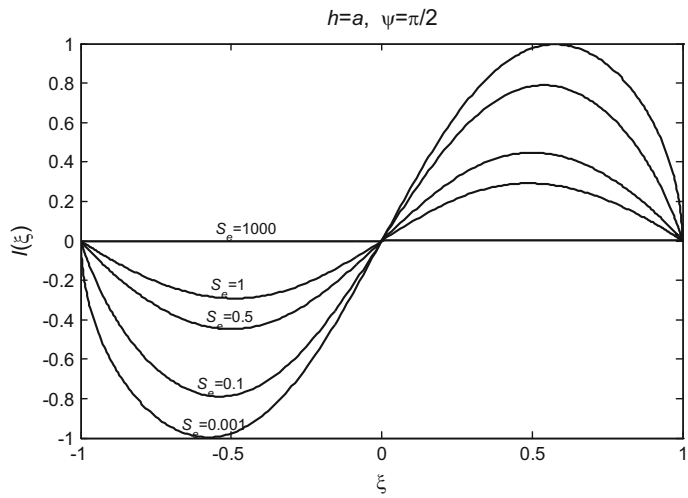

FIG. 8. Distribution of $I(\xi)$ for different values of S_e with $\hat{h} = 1$ and $\psi = \pi/2$.

is less than $\pi/2$ for $S_e = 0.1, 0.5, 1$ and is almost $\pi/2$, which is the value for a crack without surface elasticity, for $S_e = 0.001 \approx 0$. The distributions of $I(\xi)$ for $S_e = 0.001$ in Figs. 6 and 8 match quite well the exact solution in Eq. (49) for $S_e = 0$, whereas those of $\hat{f}(\xi)$ for $S_e = 1000$ in Figs. 7 and 9 match quite well the exact solution in Eq. (52) for $S_e \to \infty$.

7. Conclusions

In this work, the Gurtin–Murdoch model has been incorporated into the analysis of a mode III arc-shaped crack. First, a linear fractional transformation (11) is introduced to map the arc crack onto a straight slit in the ξ-plane. Second, the boundary value problem is formulated in the ξ-plane by considering a distribution

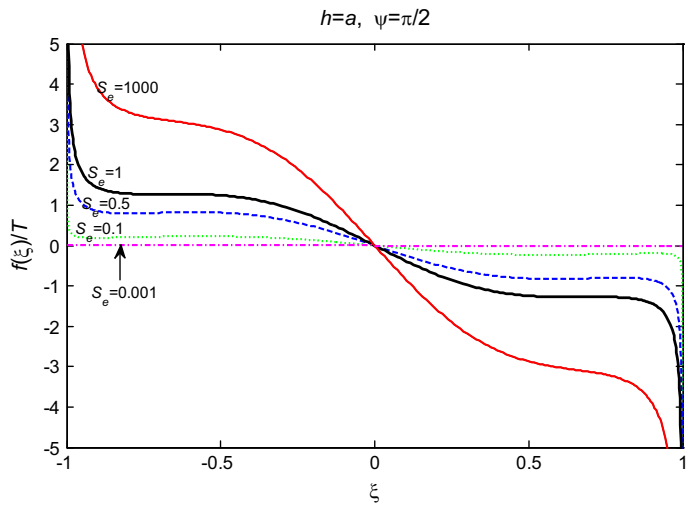

FIG. 9. Distribution of $\hat{f}(\xi)$ for different values of S_e with $\hat{h} = 1$ and $\psi = \pi/2$.

of line dislocations and line forces on the straight slit and is finally reduced to two decoupled first-order Cauchy singular integro-differential equations in Eqs. (20) and (22). The Chebyshev polynomials and collocation method are then utilized to numerically solve Eqs. (20) and (22). The analysis indicates that (i) the near-tip stresses exhibit both logarithmic and square root singularities; (ii) σ_{3n} outside the arc crack only exhibits the logarithmic singularity, σ_{3n} on the crack surfaces only exhibits the square root singularity; and (iii) σ_{3t} outside the arc crack only exhibits square root singularity, whereas σ_{3t} on the crack surfaces are bounded. Numerical results are presented to illustrate the effects of the geometric parameter $\hat{h}$, the size-dependent parameter S_e and the loading phase angle ψ on the two functions $I(\xi)$ and $\hat{f}(\xi)$.

Acknowledgments

The author is greatly indebted to two referees for their very helpful comments and suggestions. This work is supported by the National Natural Science Foundation of China (Grant No: 11272121).

References

1. Antipov, Y.A., Schiavone, P.: Integro-differential equation for a finite crack in a strip with surface effects. Q. J. Mech. Appl. Math. **64**, 87–106 (2011)
2. Chen, T., Dvorak, G.J., Yu, C.C.: Size-dependent elastic properties of unidirectional nano-composites with interface stresses. Acta Mech. **188**, 39–54 (2007)
3. Gurtin, M.E., Murdoch, A.: A continuum theory of elastic material surfaces. Arch. Ration. Mech. Anal. **57**, 291–323 (1975)
4. Gurtin, M.E., Murdoch, A.I.: Surface stress in solids. Int. J. Solids Struct. **14**, 431–440 (1978)
5. Gurtin, M.E., Weissmuller, J., Larche, F.: A general theory of curved deformable interface in solids at equilibrium. Philos. Mag. A **78**, 1093–1109 (1998)
6. Kim, C.I., Ru, C.Q., Schiavone, P.: A clarification of the role of crack-tip conditions in linear elasticity with surface effects. Math. Mech. Solids **18**, 59–66 (2013)
7. Kim, C.I., Schiavone, P., Ru, C.Q.: The effects of surface elasticity on an elastic solid with mode-III crack: complete solution. ASME J. Appl. Mech. **77**, 021011-1–021011-7 (2010a)

8. Kim, C.I., Schiavone, P., Ru, C.Q.: Analysis of a mode III crack in the presence of surface elasticity and a prescribed non-uniform surface traction. Z. Angew. Math. Phys. **61**, 555–564 (2010b)
9. Kim, C.I., Schiavone, P., Ru, C.Q.: Analysis of plane-strain crack problems (mode I and mode II) in the presence of surface elasticity. J. Elast. **104**, 397–420 (2011a)
10. Kim, C.I., Schiavone, P., Ru, C.Q.: The effects of surface elasticity on mode-III interface crack. Arch. Mech. **63**, 267–286 (2011b)
11. Kim, C.I., Schiavone, P., Ru, C.Q.: Effect of surface elasticity on an interface crack in plane deformations. Proc. R. Soc. Lond. A **467**, 3530–3549 (2011c)
12. Lengyel, T.H., Schiavone, P.: Displacement field in an elastic solid with mode-III crack and first-order surface effects. J. Mech. Mater. Struct. **7**(8), 783–794 (2012)
13. Markenscoff, X., Dundurs, J.: Annular inhomogeneities with eigenstrain and interphase modeling. J. Mech. Phys. Solids **64**, 468–482 (2014)
14. Ru, C.Q.: Simple geometrical explanation of Gurtin–Murdoch model of surface elasticity with clarification of its related versions. Sci. China **53**, 536–544 (2010)
15. Sigaeva, T., Schiavone, P.: The effect of surface stress on an interface crack in linearly elastic materials. Math. Mech. Solids (2014). doi:10.1177/1081286514534871
16. Steigmann, D.J., Ogden, R.W.: Plane deformations of elastic solids with intrinsic boundary elasticity. Proc. R. Soc. Lond. A. **453**, 853–877 (1997)
17. Walton, J.R.: A note on fracture models incorporating surface elasticity. J. Elast. **109**, 95–102 (2012)
18. Zemlyanova, A.Y.: Curvilinear mode-I/mode-II interface fracture with a curvature-dependent surface tension on the boundary. arXiv preprint arXiv:1409.3501 (2014)
19. Zemlyanova, A.Y., Walton, J.R.: Modeling of a curvilinear planar crack with a curvature-dependent surface tension. SIAM J. Appl. Math. **72**, 1474–1492 (2012)

Xu Wang
School of Mechanical and Power Engineering
East China University of Science and Technology
130 Meilong Road, Shanghai 200237, China
e-mail: xuwang@ecust.edu.cn

(Received: October 25, 2014; revised: October 31, 2014)